now published in Biochemistry,50, 6994-7001(2011)

Structural Role of Compensatory Aminoacid Replacements in the Alpha-Synuclein Protein

Valeria Losasso[1,2] ¶, Adriana Pietropaolo[3] ¶, Claudio Zannoni[4], Stefano Gustincich*[1], Paolo Carloni*[2]

¶ VL, AP contributed equally.

* Tel +49-2461-61-8941; Fax +49-2461-61-8942; email p.carloni@grs-sim.de

* Tel +39-040-3787-705; Fax +39-040-3787-702; email gustinci@sissa.it

1.International School for Advanced Studies (SISSA), 34136 Trieste, Italy

2.German Research School for Simulation Sciences GmbH, 52425 Jülich, Germany

3.Università di Catanzaro, Dipartimento di Scienze Farmacobiologiche, 88100 Catanzaro, Italy

4.Università di Bologna, Dipartimento di Chimica Fisica ed Inorganica 40136 Bologna, Italy

Abbreviations and Textual Footnotes

[1] Abbreviations: PD, Parkinson's Disease; huAS(wt), human wild type alpha-synuclein; huAS(A53T), human alpha synuclein carrying the A53T mutation; mAS(wt), mouse alpha synuclein; NMR, nuclear magnetic resonance; NAC, non-amyloid component region; CD, circular dichroism; FRET, fluorescence resonance energy transfer; SMF, single molecule force spectroscopy; MD, molecular dynamics; SASA, solvent-accessible surface area.

[2] MD studies of the protein in micelles point to a lower degree of flexibility of huAS(A53T) with respect to the huAS(wt) *(39)*. MD studies of the protein in lipid bilayer provide also interesting insights on the wild type structures, suggesting in particular that the truncated protein (residues 1–95) forms a bent helix due to its collective motions *(40)*, and that the truncated fragment (residues 31−52) assumes a high degree of conformational disorder *(41)*.

[3] NMR has provided insights of the protein in the solid state at 263 K *(42)*. mAS(wt) was found to lose transient contacts C/NAC and C/N-terminal contacts. The N-terminal domain was more rigid and the NAC region more solvent exposed relative to that of huAS(wt).

Abstract

A subset of familial Parkinson's Disease (PD) cases is associated with the presence of disease-causing point mutations in human α-synuclein (huAS(wt)), including A53T. Surprisingly, the human neurotoxic aminoacid 53T is present in non-primate, wild-type sequences of α-synucleins, including that expressed by mice (mAS(wt)). Since huAS(A53T) causes neurodegeneration when expressed in rodents, the aminoacid changes between the wild-type human protein (huAS(wt)) and mAS(wt) might act as intramolecular suppressors of A53T toxicity in the mouse protein, restoring its physiological structure and function. The lack of structural information for mAS(wt) in aqueous solution has prompted us to carry out a comparative molecular dynamics study of huAS(wt), huAS(A53T) and mAS(wt) in water at 300 K. The calculations are based on an ensemble of NMR-derived huAS(wt) structures. huAS(A53T) turns out to be more flexible and less compact than huAS(wt). Its central (NAC) region, involved in the fibril formation of the protein, is more solvent-exposed than that of the wild-type protein, in agreement with NMR data. The compactness of mAS(wt) is similar to that of the human protein. In addition, its NAC region is less solvent-exposed and more rigid than that of huAS(A53T). All of these facets may be caused by an increase of intramolecular interactions on passing from huAS(A53T) to mAS(wt). We conclude that the presence of 'compensatory replacements' in the mouse protein causes a significant change of the protein relative to huAS(A53T), restoring features not too dissimilar to those of the human protein.

Parkinson's disease (PD) is a neurodegenerative disease affecting about five million people worldwide *(1)*. In post-mortem brains of sporadic PD patients, proteinaceous fibrillar aggregates, called Lewy bodies, represent the neuropathological hallmark of the disease. The major components of Lewy bodies are fibrils of human α-synuclein (huAS(wt)) *(2)* whose function is not fully elucidated *(3)*.

HuAS(wt) exists both in cytosol and bound to the membrane *(4)*. Whilst it assumes a partially helical conformation in micelles *(5)*, NMR *(6-8)*, electron and fluorescence microscopy *(9)* and circular dichroism (CD) *(10-12)* showed that huAS(wt) is a naturally unfolded protein in aqueous solution (Figure 1b) where it may establish long range interactions. *In vitro* and *in vivo* huAS(wt) fibrillates forming a heterogeneous set of amyloid-like filaments and oligomers that are intimately involved in pathogenesis *(10, 13)*.

HuAS(wt) features three domains (Figure 1a): The N-terminal (aminoacids 1-60) amphipathic domain contains four 11-residue imperfect repeats. The (61-95) hydrophobic domain contains two additional repeats and the amyloidogenic NAC (Non Amyloid- Component) region. The hydrophobic residues 71-82 of this region are involved in the conversion into fibrillar species *(14, 15)*. Indeed, fluorimetry, electron microscopy, immuno-electron microscopy and circular dichroism spectroscopy *(15-18)* have shown that these residues are crucial for fibril formation. In addition, deletion of residues 76 and 77 strongly impairs aggregation *(18)*.

The SNCA gene coding for AS *(19)* has been found mutated in rare familial cases of PD. Together with pathological duplications, three point mutations, A30P *(20)*, E46K

(21) and A53T *(22)*, have been identified. Interestingly, the latter two fibrillate in vitro faster than huAS(wt) *(23, 24)*, whilst huAS(A30P) fibrillates slower *(23)*. In the resulting fibrils, the C-terminal domain of huAS(A53T) is more compact than that of huAS(wt), as revealed by solid-state NMR spectroscopy as well as electron and atomic force microscopy *(23, 25-26)*.

A30P and E46K mutations involve conserved aminoacids across all species as expected for a disease-provoking mutation (Figure S1). Instead, A53 is not evolutionary conserved *(22)*. Intriguingly, in non-Primate mammals, A is replaced by T, that is the familial mutation in PD. 53T is accompanied by as many as six other substitutions in mouse and rat, seven in horse. Because huAS(A53T) causes neurodegeneration when expressed in rodents *(19, 27-32)*, some of the additional substitutions (S87N, L100M, N103G, A107Y, D121G and N122S in Figure 1a) might have a compensatory effect on A53T, restoring its physiological behavior. Such behavior might arise from several factors. These might include changes of post-translation modifications, such as the loss of phosphorylation at position 87 *(33)* caused by S87N mutation. Indeed, S87 phosphorylation occurs in vivo within Lewy bodies. It is increased in brains of transgenic (TG) models of synucleinopathies and human post-mortem brains from several neurodegenerative diseases but not from normal controls *(33)*. This compensatory behavior could also arise, at least in part, from changes in structural features of the protein. These changes are the focus of the present studies.

So far biophysical methods have provided important insights on the differences between the wild-type protein and the A53T variants.

A53T causes a detachment in the NAC region in the phospholipid-bound form, which then becomes solvent-exposed *(34)*. Furthermore, it causes an overall increase in extended structure in aqueous solution relative to the wild-type protein *(35)*. As observed by NMR *(36)*, FRET *(37)* and SMF *(38)* experiments, long-range interactions present in huAS(wt) are lost. Finally, the overall flexibility of the protein increases *(36)*. It is thus clear that A53T affects huAS(wt) structure and plasticity both in solution and when bound to the phospholipids *(35, 36)*[2]. Therefore, one might expect that 'compensatory' changes in the mouse a-synuclein (mAS(wt)) primary sequence restore the physiological structure and plasticity of huAS(wt) in presence of 53T. Unfortunately, the lack of structural information of mAS(wt) in water solution and/or anchored to the membrane[3], has so far not answered the key question: does mAS(wt) share structural determinants with huAS(wt) whilst differing significantly from the disease-linked variant?

To explore the structural role of the compensatory aminoacid changes in mice, we perform a comparative sub-microsecond molecular dynamics (MD) simulation study of huAS(wt), huAS(A53T) and mAS(wt). We focus on the protein in aqueous solution because the detailed NMR-derived structures of huAS(wt) have been determined *(6, 8)*. These are here used as a starting point for this work. The study is carried out therefore in aqueous solution at 300 K. It covers overall a sub-microsecond timescale and takes advantage of the so-called chirality index analysis. This allows detecting secondary structure motifs and protein backbone flexibility, as shown already for the prion protein *(43, 44)*.

We first investigate the structural determinants of huAS(wt) and huAS(A53T) proving that our calculations based on Amber99SB force field reproduces the

experimental structural information obtained by SMF and NMR. We then take advantage of the same computational protocol to identify the structure and conformational fluctuations of mAS(wt) unveiling the role of the 'compensatory' aminoacid substitutions from human to the mouse protein to suppress the neurotoxic effect of the A53T mutation (Figure 1a).

Methods

We clustered the huAS(wt) ensemble obtained by NMR data using the algorithm from *(45)*, with a cutoff of 22 Å. This cutoff corresponds to the maximum of the Gaussian-like shape of the C_α carbons RMSD (root mean square distance) distribution, calculated over each pair combination of conformations. In this way, we obtained 23 clusters. The first six of them, covering 73% of the conformations, were selected. The former have population 0.4, 0.12, 0.07, 0.06, 0.04 and 0.04. Six huAS(A53T) conformers were constructed by replacing A53 with T and, in the case of mAS(wt), also S87 with N, L100 with M, N103 with G, A107 with Y, D121 with G and N122 with S, in the six representatives of huAS(wt). The Swiss-PdbViewer program was used *(46)*. The 18 systems were inserted in a water box. The size of the water box was chosen in order to have a minimum distance of 10 Å between any atom and the edge of the box. The number of added water molecules varied largely (between ~25000 and ~60000), according to the compactness of the structure. 9, 9 and 8 Na^+

counterions were added to neutralize the huAS(wt), huAS(A53T) and mAS(wt) systems, respectively.

The AMBER ff99SB *(47)*, the Aaqvist *(48)* and the TIP3P *(49)* force fields were used for the protein, the sodium ions and water, respectively. Periodic boundary conditions were applied. Electrostatic interactions were calculated using the Particle Mesh Ewald method *(50)*. The time-step was set to 2 fs. The SHAKE algorithm *(51)* was applied to fix all bond lengths. A cutoff distance of 10 Å was used for electrostatic and van der Waals interactions. Room conditions (T = 300 K and P = 1,013 bar) were achieved by coupling the systems with a Langevin thermostat *(52)* with a coupling coefficient of 5 ps, and a Nosé-Hoover Langevin barostat *(53)* with an oscillation period of 200 fs and the damping timescale of 100 fs. 40 ns of MD for each of the six clusters were carried out for huAS(wt), huAS(A53T) and mAS(wt) for a total of 0.72 μs using the NAMD 2.7 package *(54)*.

Several properties were calculated on the equilibrated MD structures (see SI for details): (i) The normalized average C_α-C_α contact maps. (ii) The normalized aromatic stacking maps, defined in terms of Y/F rings' centers of mass distances and the angle formed by the two vectors along the C_2 axis of the F/Y benzyl moieties. (iii) Salt-bridges, which are assumed to exist if the distance between the R-NH_3^+ groups of Lysines and R-COO^- groups of Glutamates and Aspartates is less than 3.5 Å. (iv) The average gyration radius, which is calculated as in ref. *(55)*. (v) The CD spectrum, which is calculated using the DichroCalc program suite *(56)* considering the semi-empirical parameters of *(57)*. It is averaged according to the population of huAS(wt) representative clusters *(58)*. It is reported for all the representative clusters in

huAS(A53T) and mAS because for the latter the contribution of each representative to the contribution of the ensemble of structures of the proteins are not known, in contrast to that of HuAS(wt). (vi) The intensity ratios for huAS(wt). These are the ratios of crosspeak intensities in the spectra of the oxidized and reduced states of the spin-label MTSL as a function of residue number. They have been measured for selected cysteine mutants, namely 24, 42, 62, 87 and 103. These were calculated using the formula of ref. *(59)*. (vii) The solvent exposure of the NAC domain in terms of the solvent accessible surface area (SASA), calculated as in *(60)*. (viii) The backbone local flexibility content, which is calculated based on the so-called chirality index per residue G and its standard deviations (σG) *(43, 61-62)*. An increase of σG indicates increased flexibility *(44)*. (ix) The normalized correlation functions for pairs of residues undergoing substitutions. These involve different residues or the same residue, e.g. A53T-S87N, A53T-A53T). They were calculated as a function of time based on the chirality indexes. As usual, full correlation occurs when the function is equal to 1. A decrease of this value points to a decreased correlation. From those we obtain the 1/t quantity defined in the Results Section.

Results

Six representatives (1-6) (Figure 1b) of huAS(wt) NMR structures were investigated with Amber99SB force field based-MD simulations. These representatives were extracted by cluster analysis *(45)* from the ensemble of 4,000 structures revealed by NMR spectroscopy *(8)*. They represent 73% of conformations. They have been previously used to investigate the binding of dopamine and dopamine derivatives to huAS(wt) *(63, 64)*. Overall, calculations are carried out for 0.24 microseconds. As shown in Table 1, the calculated average gyration radii for 1 to 6 were respectively

25, 28, 27, 38, 21 and 43 Å. These are similar to those of initial NMR structures (Table 1). Contact maps are presented in Figure 2a. These results are consistent with NMR data that identified compact and unordered conformations with average gyration radii values of 24.7 Å and 41.9 Å *(6, 8)*.

According to our calculations, conformers are classified in three classes (Figure 1c). One class, derived from conformers 1 and 5, includes conformations with long-range packing. The second class, derived from conformers 2, 4 and 6, are random coil. The last class, derived from conformer 3, features β-like structures. The presence of these classes is fully consistent with evidence from single molecule force spectroscopy (SMF) experiments *(65)*.

Contact maps identified N-terminal/C-terminal and NAC/C-terminal long-range interactions. Contacts were present for residues 60-80 with 120-140, as well as for the 80-90 domain with the 120-140 region (Figure 2a). This result is consistent with NMR data *(6, 8)* as well as with OPLS-based MD simulations starting from the completely stretched structure of the protein *(66)*.

We calculated the CD spectrum (Figure S2). This reproduces the one obtained experimentally *(11, 12)* and indicates a large presence of random coil structure.

Finally, we calculated the so called 'intensity ratios' *(8, 59) (*Figure S3 in Supplementary Material). These are the ratios of crosspeak intensities in the spectra of the oxidized and reduced states of the spin-label MTSL as a function of residue number. They have been measured for cysteine mutations of residues 24, 42, 62, 87 and 103 (8). The calculated values are in good agreement with the experimental data *(8)* (See Caption of Fig. S3 for more details).

We then compare our computational predictions on huAS(wt) with those on huAS(A53T). To this purpose we took advantage of available SMF and NMR experimental data for the human mutant protein.

First, the N-terminal/C-terminal and NAC/C-terminal long-range interactions present in huAS(A53T) are lost. The average gyration radii of most conformers are larger than the corresponding ones in huAS(wt), pointing to an overall decrease of compactness (Table 1). This is also observed by visual inspection of the structure Figure 1b). These results are consistent with NMR data, which showed the absence of long-range contacts in huAS(A53T) and the presence of a rather extended structure *(35, 36)*. These findings are also consistent with SMF experiments, which demonstrated that huAS(A53T) exhibits a limited mechanical resistance to unfolding *(38)*. Interestingly, the calculated solvent accessible surface area (SASA) of the NAC region is larger than in huAS(wt) (Figure 2b). This finding is also consistent with NMR data *(36)*. Finally, the overall flexibility of the mutant (especially in its NAC region) is larger than that of huAS(wt), as shown by the calculation of the standard deviation of the chirality index (σG in Figure 3, see SI for details) and by NMR data *(36)*. In our calculations, the increase in SASA and the flexibility of the NAC region in huAS(A53T) is caused by the loss of NAC/C-terminal interactions (Figure 2b) that shield and render more rigid the NAC region of huAS(wt).

We thus conclude that our simulation protocol reproduces all known structure and plasticity properties of huAS(wt) and huAS(A53T).

We then apply the same computational set up to analyze mAS(wt). This features the A53T along with the S87N, L100M, N103G, A107Y, D121G and N122S substitutions.

As shown in Figure 2 c), mAS(wt) adopts two separately packed domains, the N- and the C-terminal cores. As a result, the compactness of the structure is not too dissimilar from that of huAS(wt), as shown by the calculation of the gyration radii (Table 1) and of the contact maps (Figure 2a)[3]. The C-terminal and, more strongly, the N-terminal cores are stabilized by intradomain salt bridges (Table S2). The SASA of the NAC region is smaller than that of huAS(A53T) (Figure 2b).

Interestingly, the flexibility of mAS(wt) (and in particular of the NAC region) is comparable to that of huAS(wt) and smaller than that of huAS(A53T) (Figure 3). The smaller flexibility of the C-terminal relative to huAS(A53T) is likely to be caused by intramolecular interactions that are not present in huAS(A53T) (Figure 2a). These include: (i) the π-stacking interactions between the aromatic rings of Y133 and Y136 (Figure S4); (ii) the N87-E83 H-bond, which bridges the NAC region to the upstream region of the C-terminal domain (Figure 2a).

Insights on the flexibility of the residues undergoing substitutions are obtained from an analysis of the correlation functions among the backbone atoms of these residues. These functions represent the correlation between the instantaneous chirality of different residues. Figure S5 shows an example of those. Constant values of such correlation indicate low relative flexibility (see Methods). Within a certain timescale τ, this function will vary by 100% of its initial value. We may say then that the original correlation is then practically lost. We therefore use the reciprocal of this quantity ($1/\tau$) as another index for flexibility that can change the local chirality (Table 2).

The $1/\tau$ values are larger for the disease-linked variant than those of the other two proteins. This points to a larger flexibility of the residue undergoing substitutions in

huAS(A53T). A consistent picture is obtained by analyzing the flexibility indexes previously defined in terms of standard deviations of chirality indexes (Tables S3-S5). Furthermore the residues undergoing substitutions in the C-terminal of huAS(wt) and huAS(A53T) are more flexible than those of mAS(wt). The chirality indexes analysis provides consistent results also in this case (Table S3-S5).

Discussion

The dominant mutation huAS(A53T) is responsible for a subset of familial cases of PD. The structural features of this protein have been extensively studied to better understand the structural bases of neurotoxicity. In this context, NMR data as well as SMF experiments have provided important descriptions of differences and commonalities with huAS(wt). Surprisingly, while the overexpression of huAS(A53T) in mouse may induce neurodegeneration, mAS(wt) presents an A53T substitution, similar to the pathogenic mutation in humans. It was therefore important to study the role of the six additional aminoacid changes between mouse and human primary sequences on mAS(wt) structure to identify potential intramolecolar suppressors of A53T toxicity.

Unfortunately, the lack of structural information of mAS(wt) in water solution and/or anchored to the membrane[2], has so far hampered to address this study.

Here we report a computational protocol that accurately predicts structural and plasticity properties for huAS(wt) and huAS(A53T) recapitulating NMR and SMF experimental data. To this purpose, we take advantage of the chirality index *(43, 44)*.

We then use this computational set up to predict structure and flexibility of mAS(wt).

Our calculations show that the presence of compensatory aminoacid substitutions in mAS(wt) does restore key structural aspects of huAS(wt). In particular, a variety of intramolecular interactions allow the NAC region of mAS(wt) to be significantly more compact and less flexible than in huAS(A53T). In this context, the formation of the N87-E83 H-bond, which bridges the NAC region to the upstream region of the C-terminal domain (Figure 2a) is especially relevant. Indeed S87 in huAS(wt) and in huAS(A53T) forms this H-bond neither with E83, nor with any other residues of the protein.

It is also interesting to note that E83 was previously shown to be essential in the ability of dopamine to inhibit huAS(wt) fibril formation *(63)*. We conclude that the presence of 'compensatory replacements' in the mouse protein causes a rather dramatic change of structure and plasticity of the protein, restoring structural features not too dissimilar from those of huAS(wt). Future experiments *in vivo* and *in vitro* should address the role of S87N substitution as an intramolecular suppressor of A53T toxicity.

Acknowledgments

The authors thank Michele Vendruscolo for providing them with the 4000 NMR structures of huAS(wt).

Supporting Information

Methods, supplemental tables and figures. This material is available free of charge via the Internet at http://pubs.acs.org.

References

1. Shehadeh, L.A., Yu, K., Wang, L., Guevara, A., Singer, C., Vance J., and Papapetropoulos, S. (2010) SRRM2, a potential blood biomarker revealing high alternative splicing in Parkinson's disease. *PLoS ONE 5*, e9104.

2. Spillantini, M.G., Schmidt, M.L., Lee, V.M., Trojanowski, J.Q., Jakes, R., and Goedert, M. (1997) Alpha synuclein in Lewy bodies. *Nature 388,* 839-840.

3. Bonini, N.M., and Giasson, B.I. (2005) Snaring the function of alpha synuclein. *Cell 123*, 359-361.

4. Lee, H.J., Choi, C., and Lee, S.J. (2002) Membrane-bound α-synuclein has a high aggregation propensity and the ability to seed the aggregation of the cytosolic form. *J. Biol. Chem. 277*, 671-678.

5. Ulmer, T.S. and Bax, A. (2005) Comparison of structure and dynamics of micelle-bound human alpha-synuclein and Parkinson disease variants. *J. Biol. Chem. 280*, 43179–43187.

6. Bertoncini, C.W., Jung, Y.S., Fernández, C.O., Hoyer, W., Griesinger, C., Jovin, T.M., and Zweckstetter, M. (2005) Release of long-range tertiary interactions potentiates aggregation of natively unstructured alpha-synuclein. *Proc. Natl. Acad. Sci. U.S.A. 102*, 1430-1435.

7. Rasia, R.M., Bertoncini, C.W., Marsh, D., Hoyer, W., Cherny, D., Zweckstetter, M., Griesinger, C., Jovin, T.M., and Fernández, C.O. (2005) Structural characterization of copper(II) binding to alpha-synuclein: insights into the bioinorganic chemistry of Parkinson's disease. *Proc. Natl. Acad. Sci. U.S.A. 102*, 4294–4299.

8. Dedmon, M.M., Lindorff-Larsen, K., Christodoulou, J., Vendruscolo, M., and Dobson, C.M. (2005) Mapping long-range interactions in alpha-synuclein using spin-label and ensemble molecular dynamics simulations. *J. Am. Chem. Soc. 127,* 476–477.

9. Hoyer, W., Cherny, D., Subramaniam, V., and Jovin, T.M. (2004) Impact of the acidic C-terminal region comprising amino acids 109-140 on alpha-synuclein aggregation in vitro. *Biochemistry 43,* 16233-16242.

10. Hong, D.P., Xiong, W., Chang, J.Y., and Jiang, C. (2011) The role of the C-terminus of human alpha-synuclein: intra-disulfide bonds between the C-terminus and other regions stabilize non-fibrillar monomeric isomers. *FEBS Lett. 585,* 561-566.

11. Eliezer, D., Kutluay, E., Bussell, R., and Browne, G. (2001) Conformational properties of alpha-synuclein in its free and lipid-associated states. *J. Mol. Biol. 307,* 1961-1973.

12. Maiti, N.C., Apetri, M.M., Zagorski, M.H., Carey, P.R., and Anderson, V.E. (2004) Raman spectroscopic characterization of secondary structure in natively unfolded protein: alpha-synuclein. *J. Am. Chem. Soc. 126,* 2399-2408.

13. Murray, I.V.J., Giasson, B.I., Quinn, S.M., Koppaka, V., Axelsen, P.H., Ischiropoulos, H., Trojanowsky, J.Q., and Lee, V.M. (2003) Role of α-synuclein carboxy-terminus on fibril formation in vitro. *Biochemistry 42*, 8530–8540.

14. Bodles, A.M., Guthrie, D.J., Greer, B., and Irvine, G.B. (2001) Identification of the region of non-Abeta component (NAC) of Alzheimer's disease amyloid responsible for its aggregation and toxicity. *J. Neurochem. 78*, 384–395.

15. Giasson, B.I., Murray, I.V., Trojanowski, J.Q., and Lee, V.M. (2001) A hydrophobic stretch of 12 amino acid residues in the middle of alpha-synuclein is essential for filament assembly. *J. Biol. Chem. 276*, 2380–2386.

16. Der Sarkissian, A., Jao, C.C., Chen, J., and Langen, R. (2003) Structural organization of alpha-synuclein fibrils studied by site-directed spin labeling. *J. Biol. Chem.* 278, 37530-37535.

17. Del Mar, C., Greenbaum, E.A., Mayne, L., Englander, S.W., and Woods, V.L. (2005). Structure and properties of α-synuclein and other amyloids determined at the amino acid level. *Proc. Natl. Acad. Sci*. 102, 15477-15482.

18. Waxman E.A., Mazzulli J.R., and Giasson B.I. (2009) Characterization of hydrophobic residue requirements for alpha-synuclein fibrillization. *Biochemistry* 48, 9427-9436.

19. Shulman, J.M., De Jager, P.L., and Feany, M.B. (2011) Parkinson's disease: genetics and pathogenesis. *Annu, Rev. Pathol, 6*, 193-222.

20. Kruger, R., Kuhn, W., Muller, T., Woitalla, D., Graeber, M., Kösel, S., Przuntek, H., Epplen, J.T., Schöls, L., and Riess, O. (1998) Ala30Pro mutation in the gene encoding α-synuclein in Parkinson's disease. *Nat. Genet. 18*, 106–108.

21. Zarranz, J.J., Alegre, J., Gomez-Esteban, J.C., Lezcano, E., Ros, R., Ampuero, I., Vidal, L., Hoenicka, J., Rodriguez, O., Atares, B., Llorens, V., Gomez Tortosa, E., del Ser, T., Munoz, D.G. and de Yebenes, J.G. (2004) The new mutation, E46K, of alpha-synuclein causes Parkinson and Lewy-body dementia. *Ann. Neurol. 55*, 164-173.

22. Polymeropoulos, M.H., Lavedan, C., Leroy, E., Ide, S.E., Dehejia, A., Dutra, A., Pike, B., Root, H., Rubenstein, J., Boyer, R., Stenroos, E.S., Chandrasekharappa, S., Athanassiadou, A., Papapetropoulos, T., Johnson, W.G., Lazzarini, A.M., Duvoisin, R.C., Di Iorio, G., Golbe, L.I., and Nussbaum, R.L. (1997) Mutation in the alpha-synuclein gene identified in families with Parkinson's disease. *Science 276,* 2045-2047.

23. Conway, K.A., Harper, J.D., and Lansbury, P.T. (1998) Accelerated in vitro fibril formation by a mutant alpha-synuclein linked to early-onset Parkinson disease. *Nat. Med. 4,* 1318-1320.

24. Fredenburg, R.A., Rospigliosi, C., Meray, R.K., Kessler, J.C., Lashuel, H.A., Eliezer, D., and Lansbury, P.T. (2007) The impact of the E46K mutation on the properties of alpha synuclein in its monomeric and oligomeric states. *Biochemistry 46,* 7107-1118.

25. Heise, H., Celej, M.S., Becker, S., Riedel, D., Pelah, A., Kumar, A., Jovin, T.M., and Baldus, M. (2003) Solid-state NMR reveals structural differences between fibrils of wild-type and disease-related A53T mutant alpha-synuclein. *J. Mol. Biol. 380*, 444-450.

26. Suk, J.E., Lokappa, S.B., and Ulmer, T.S. (2010) The clustering and spatial arrangement of beta-sheet sequence, but not order, govern alpha-synuclein fibrillogenesis. *Biochemistry 49*, 1533-1540.

27. Graham, D.R. and Sidhu, A. (2010) Mice expressing the A53T mutant form of human alpha-synuclein exhibit hyperactivity and reduced anxiety-like behavior. *J. Neurosci. Res. 88*, 1777-1783.

28. Giasson, B.I., Duda, J.E., Quinn, S.M., Zhang, B., Trojanowski, J.Q., and Lee, V.M. (2002) Neuronal α-synucleinopathy with severe movement disorder in mice expressing A53T human α-synuclein. *Neuron 34*, 521-533.

29. Koprich, J.B., Johnston, T.H., Reyes, M.G., Sun, X., and Brotchie, J.M. (2010) Expression of human A53T alpha-synuclein in the rat substantia nigra using a novel AAV1/2 vector produces a rapidly evolving pathology with protein aggregation, dystrophic neurite architecture and nigrostriatal degeneration with potential to model the pathology of Parkinson's disease. *Mol. Neurodegen. 5*, 43.

30. Tsika, E., Moysidou, M., Guo, J., Cushman, M., Gannon, P., Sandaltzopoulos, R., Giasson, B.I., Krainc, D., Ischiropoulos, H., and Mazzulli, J.R. (2010) Distinct region-specific alpha-synuclein oligomers in A53T transgenic mice: implications for neurodegeneration. *J. Neurosci. 30*, 3409-3418.

31. Gispert, S., Del Turco, D., Garrett, L., Chen, A., Bernard, D.J., Hamm-Clement, J., Korf, H.W., Deller, T., Braak, H., Auburger, G., and Nussbaum, R.L. (2003) Transgenic mice expressing mutant A53T human alpha-synuclein show neuronal dysfunction in the absence of aggregate formation. *Mol. Cell. Neurosci. 24*, 419-429.

32. Kurz, A., Double, K.L., Lastres-Becker, I., Tozzi, A., Tantucci, M., Bockhart, V., Bonin, M., García-Arencibia, M., Nuber, S., Schlaudraff, F., Liss, B., Fernández-Ruiz, J., Gerlach, M., Wüllner, U., Lüddens, H., Calabresi, P., Auburger, G., and Gispert, S. (2010) A53T-alpha-synuclein overexpression impairs dopamine signaling and striatal synaptic plasticity in old mice. *PLoS ONE 5*, e11464.

33. Paleologou, K.E., Oueslati, A., Shakked, G., Rospigliosi, C.C., Kim, H.Y., Lamberto, G.R., Fernández, C.O., Schmid, A., Chegini, F., Gai, W.P., Chiappe, D., Moniatte, M., Schneider, B.L., Aebischer, P., Eliezer, D., Zweckstetter, M., Masliah, E., and Lashuel, H.A. (2010) Phosphorylation at S87 is enhanced in synucleinopathies, inhibits alpha-synuclein oligomerization, and influences synuclein-membrane interactions. *J. Neurosci. 30,* 3184-3198.

34. Bodner, C.R., Maltsev, A.S., Dobson, C.M., and Bax, A. (2010) Differential phospholipid binding of AS variants implicated in Parkinson's Disease revealed by solution NMR spectroscopy. *Biochemistry 49*, 862-871.

35. Bussell, R., and Eliezer, D. (2001) Residual structure and dynamics in Parkinson's disease-associated mutants of alpha-synuclein. *J. Biol. Chem. 276*, 45996-46003.

36. Bertoncini, C.W., Fernández, C.O., Griesinger, C., Jovin, T.M., and Zweckstetter, M. (2005) Familial mutants of alpha-synuclein with increased neurotoxicity have a destabilized conformation. *J. Biol. Chem. 280,* 30649-30652.

37. Lee, J.C., Langen, R., Hummel, P.A., Gray, H.B., and Winkler, J.R. (2004) Alpha-synuclein structures from fluorescence energy-transfer kinetics: implications for the role of the protein in Parkinson's disease. *Proc. Natl. Acad. Sci. U.S.A.* 101, 16466–16471.

38. Brucale, M., Sandal, M., Di Maio, S., Rampioni, A., Tessari, I., Tosatto, L., Bisaglia, M., Bubacco, L., and Samorì, B. (2009) Pathogenic mutations shift the equilibria of alpha-synuclein single molecules towards structured conformers. *Chembiochem. 10*, 176-183.

39. Perlmutter, J.D., Braun, A., and Sachs, J.N. (2009) Curvature dynamics of alpha-synuclein familial Parkinson disease mutants: molecular simulations of the micelle- and bilayer-bound forms. *J. Biol. Chem. 284*, 7177-7189.

40. Mihajlovic. M., and Lazaridis, T. (2008) Membrane-bound structure and energetics of alpha-synuclein. *Proteins 70*, 761-768.

41. Bortolus, M., Tombolato, F., Tessari, I., Bisaglia, M., Mammi, S., Bubacco, L., Ferrarini, A., and Maniero, A.L. (2008) Broken helix in vesicle and micelle-bound alpha-synuclein: insights from site-directed spin labeling-EPR experiments and MD simulations. *J. Am. Chem. Soc. 130*, 6690-6691.

42. Wu, K.P., Kim, S., Fela, D.A., and Baum, J. (2008) Characterization of conformational and dynamic properties of natively unfolded human and mouse alpha-synuclein ensembles by NMR: implications for aggregation. *J. Mol. Biol. 378*, 1104-1115.

43. Pietropaolo, A., Muccioli, L., Berardi, R., and Zannoni, C. (2008) A chirality index for investigating protein secondary structures and their time evolution. *Proteins 70,* 667–677.

44. Pietropaolo, A., Muccioli, L., Zannoni, C., and Rizzarelli, E. (2009) Conformational preferences of the full chicken prion protein in solution and its differences with respect to mammals. *ChemPhysChem. 10*, 1500-1510.

45. Micheletti, C., Seno, F., and Maritan, A. (2000) Recurrent oligomers in proteins: an optimal scheme reconciling accurate and concise backbone representations in automated folding and design studies. *Proteins 40*, 662-674.

46. Guex, N., and Peitsch, M.C. (1997) SWISS-MODEL and the Swiss-PdbViewer: an environment for comparative protein modeling. *Electrophoresis. 18*, 2714-2723.

47. Hornak, V., Abel, R., Okur, A., Strockbine, B., Roitberg, A., and Simmerling, C. (2006) Comparison of multiple Amber force fields and development of improved protein backbone parameters. *Proteins 65*, 712–725.

48. Aaqvist, J. (1990) Ion-water interaction potentials derived from free energy perturbation simulations. *J. Phys. Chem. 94*, 8021-8024.

49. Jorgensen, W.L., Chandrasekhar, J., Madura, J.D., Impey, R.W., and Klein, M.L. (1983) Comparison of simple potential functions for simulating liquid water. J. *Chem. Phys. 79*, 926-935.

50. Darden, T., York, D., and Pedersen, L. (1993) Particle mesh Ewald: An N-log(N) method for Ewald sums in large systems. *J. Chem. Phys. 98*, 10089-10093.

51. Ryckaert, J.P., Ciccotti, G., and Berendsen, H.J.C. (1977) Numerical integration of the cartesian equations of motion of a system with constraints: molecular dynamics of n-alkanes. *J. Comp. Phys. 23*, 327–341.

52. Adelman, S.A., and Doll, J.D. (1976) Generalized langevin equation approach for atom/solid surface scattering: general formulation for classical scattering off harmonic solids. *J. Chem. Phys. 64*, 2375–2388.

53. Feller, S.E., Zhang, Y., Pastor, R.W., and Brooks, B.R. (1995) Constant pressure molecular dynamics simulation: the Langevin piston method. *J. Chem. Phys. 103*, 4613-4621.

54. Phylips, J.C., Braun, R., Wang, W., Gumbart, J., Tajkhorshid, E., Villa, E., Chipot, C., Skeel, R.D., Kalé, L., and Schulten, K. (2005). Scalable molecular dynamics with NAMD. *J. Comput. Chem. 26*, 1781-1802.

55. Humphrey, W., Dalke, A., and Schulten, K. (1996) VMD: visual molecular dynamics. *J. Mol. Graph. 14*, 33–38.

56. Bulheller, B.M., and Hirst, J.D. (2009) DichroCalc–circular and linear dichroism online. *Bioinformatics 25*, 539–540.

57. Sreerama, N., and Woody, R.W. (2000) Estimation of protein secondary structure from circular dichroism spectra: comparison of CONTIN, SELCON, and CDSSTR methods with an expanded reference set. *Anal. Biochem. 287*, 252-260.

58. Glättli, A., Daura, X., Seebach, D., and van Gunsteren, W.F. (2002) Can one derive the conformational preference of a β-peptide from its CD Spectrum? *J. Am. Chem. Soc 124*, 12972–12978.

59. Teilum, K., Kragelund, B.B., and Poulsen, F.M. (2002) Transient structure formation in unfolded acyl-coenzyme A-binding protein observed by site-directed spin labelling. *J. Mol. Biol. 324*, 349-357.

60. Futamura, N., Aluru, S., Ranjan, D., and Hariharan, B. (2002) Efficient parallel algorithms for solvent accessible surface area of proteins. *IEEE Trans. on Parallel and Distributed Systems 13*, 544-555.

61. Neal, M.P., Solymosi, M., Wilson, M.R., and Earl, D.J. (2003) Helical twisting power and scaled chiral indices. *J. Chem. Phys. 119*, 3567–3573.

62. Solymosi, M., Low, R.J., Grayson, M., and Neal, M.P. (2002) A generalized scaling of a chiral index for molecules. *J. Chem. Phys. 116*, 9875–9881.

63. Herrera, F.E., Chesi, A., Paleologou, K.E., Schmid, A., Munoz, A., Vendruscolo, M., Vendruscolo, M., Gustincich, S., Lashuel, H.A., and Carloni, P. (2008) Inhibition of alpha-synuclein fibrillization by dopamine is mediated by interactions with five C-terminal residues and with E83 in the NAC region. *PLoS ONE 3*, e3394.

64. Latawiec, D., Herrera, F.E., Bek, A., Losasso, V., Candotti, M., Benetti, F., Carlino, E., Kranjc, A., Lazzarino, M., Gustincich, S., Carloni, P., and Legname, G. (2010) Modulation of alpha-synuclein aggregation by dopamine analogs. *PLoS ONE 5*, e9234.

65. Sandal, M., Valle, F., Tessari, I., Mammi, S., Bergantino, E., Musiani, F., Brucale, M., Bubacco, L., and Samorì, B. (2008) Conformational equilibria in monomeric alpha-synuclein at the single-molecule level. *PLoS Biol. 6,* 99-108.

66. Wu, K.P., Weinstock, D.S., Narayanan, C., Levy, R.M., and Baum, J.B. (2009) Structural reorganization of alpha-synuclein at low pH observed by NMR and REMD simulations. *J. Mol. Biol. 391*, 784-796.

Table 1. Gyration radii (Å) for the six MD ensemble of huAS(wt), huAS(A53T) and mAS(wt)[a].

Structure number	huAS(wt)		huAS(A53T)		mAS(wt)		NMR structure
01	24.8	(7.4)	31.7	(2.8)	26.1	(5.0)	39.4
02	28.0	(4.1)	32.6	(1.6)	36.9	(2.3)	35.1
03	27.5	(3.9)	32.4	(2.9)	28.1	(4.0)	35.6
04	38.3	(5.0)	41.3	(6.8)	43.3	(2.7)	46.0
05	21.2	(2.4)	21.4	(3.0)	23.1	(3.4)	29.6
06	42.6	(5.3)	59.0	(2.5)	52.7	(4.0)	53.3

[a] Standard deviations are reported in brackets. The initial NMR values for huAS(wt) are also reported.

Table 2. $1/\tau$ values (ns^{-1}) for huAS(wt) structures (left values), huAS(A53T) structures (center values) and mAS(wt) structures (right values).[a]

Residue numbers	Structure number																	
	01			02			03			04			05			06		
53-53	0	.2	0	0	0	0	0	.2	0	0	0	0	0	.1	0	0	0	0
53-87	0	.2	.1	.1	.1	0	0	0	0	.7	.2	.1	0	0	.1	0	1	1
53-100	0	0	.1	0	.2	0	0	0	.1	.1	.2	0	0	.2	0	.7	0	0
53-103	0	0	1	0	0	1	.2	.2	.1	.2	.3	0	0	.5	0	.1	0	0
53-107	0	1	.2	.1	.1	0	0	0	0	.1	.1	.2	.1	`	0	0	0	0
53-121	0	.1	0	.5	.1	0	0	.2	.1	0	0	.1	0	0	0	0	.2	.2
53-122	0	.1	0	.2	.1	0	.5	.1	0	0	.1	0	0	.1	0	0	.5	.5
87-87	0	0	.5	0	1	.1	0	0	0	0	.1	0	0	0	.1	0	1	.5
87-100	0	.1	.1	1	.1	0	0	0	0	0	.1	.1	0	.1	0	0	1	1
87-103	0	.1	1	1	1	.1	.2	.1	.1	.1	.1	.5	.1	.1	0	.1	.5	.5
87-107	0	1	.2	.3	.1	0	.1	0	0	0	.1	1	.1	0	0	.1	.5	.5
87-121	0	.3	.1	.1	.2	0	0	0	.1	0	.1	.2	.1	0	0	.1	.5	.5
87-122	0	1	0	0	1	0	.1	.1	0	0	.1	.2	.1	.2	0	.1	1	1
100-100	0	0	1	0	.2	0	0	0	1	.1	.2	0	.1	0	0	.1	0	0
100-103	0	0	.1	0	.2	.1	.2	0	.1	.1	.1	0	.1	.1	.1	0	0	0
100-107	0	1	.1	.1	.2	0	0	0	0	0	1	.3	.1	0	0	0	0	0
100-121	0	0	.1	1	1	0	0	0	.1	0	1	0	.1	0	0	0	.1	.1
100-122	0	.2	.1	1	.1	0	.2	1	0	0	.5	0	1	.1	0	0	.2	.2
103-103	0	0	.5	.1	0	.5	.1	0	.1	.5	.3	.1	0	.3	0	0	1	0
103-107	0	1	1	.2	1	.1	.1	.1	.1	0	.1	.2	.1	.3	0	0	0	0
103-121	0	0	0	.3	.1	.1	.1	.1	.1	.1	.1	0	0	.3	.1	.1	.2	.2
103-122	0	.1	0	.5	.1	.3	.3	.2	.1	.1	1	.1	.1	1	0	.1	.1	.1
107-107	0	.2	0	0	.1	0	0	0	0	0	.2	.3	.1	0	0	0	0	0
107-121	0	.1	0	0	.1	0	0	0	0	0	0	.1	.1	0	.1	0	.2	.2
107-122	0	0	0	.1	1	0	.1	.1	0	0	.1	.5	.2	.1	0	0	.1	.1
121-121	0	0	0	.1	0	0	0	0	.1	0	0	0	0	0	0	0	.2	.2
121-122	0	.1	0	0	0	0	.1	.1	0	0	.1	0	.1	1	0	0	.2	.2
122-122	0	.2	0	.2	.2	0	.1	.1	0	0	.1	0	.1	.1	0	0	.2	.2

[a] Values corresponding to 1/t longer than the MD time window are set to 0.

Figure legends

Figure 1.

a) Sequence alignment between huAS(wt) and mAS(wt). The residues changing from one species to another are highlighted in bold. b)-d): Backbone representations of the six selected MD structures ( ) of huAS(wt) b), huAS(A53T) c) and mAS(wt) d), obtained with the procedure outlined in the text. The side chains of the hydrophobic residues of the NAC region (residues 71-82) are also displayed.

Figure 2. a) Contact maps of huAS(wt), huAS(A53T) and mAS(wt) representatives. Long range contacts are present only in huAS(wt)1, and huAS(wt)5 (the number from 1 to 6 indicate the extent of cluster population, 1 is the most populated cluster). Few extents of long range contacts are present in mAS(wt)1, mAS(wt)5 and huAS(A53T)5. The standard deviation of the values in the contact maps are reported in Fig. S6 of the Supporting Information. b) Solvent Accessible Surface Area (SASA) for the NAC region of huAS(wt), huAS(A53T) and mAS(wt).

Figure 3. Snapshots for the six MD ensembles of huAS(wt), huAS(A53T) and mAS(wt). The structures are colored according to their degree of flexibility, whose color panel is reported on the top. Structures are oriented with N-terminal on the left and C-terminal on the right.

Figure 1.

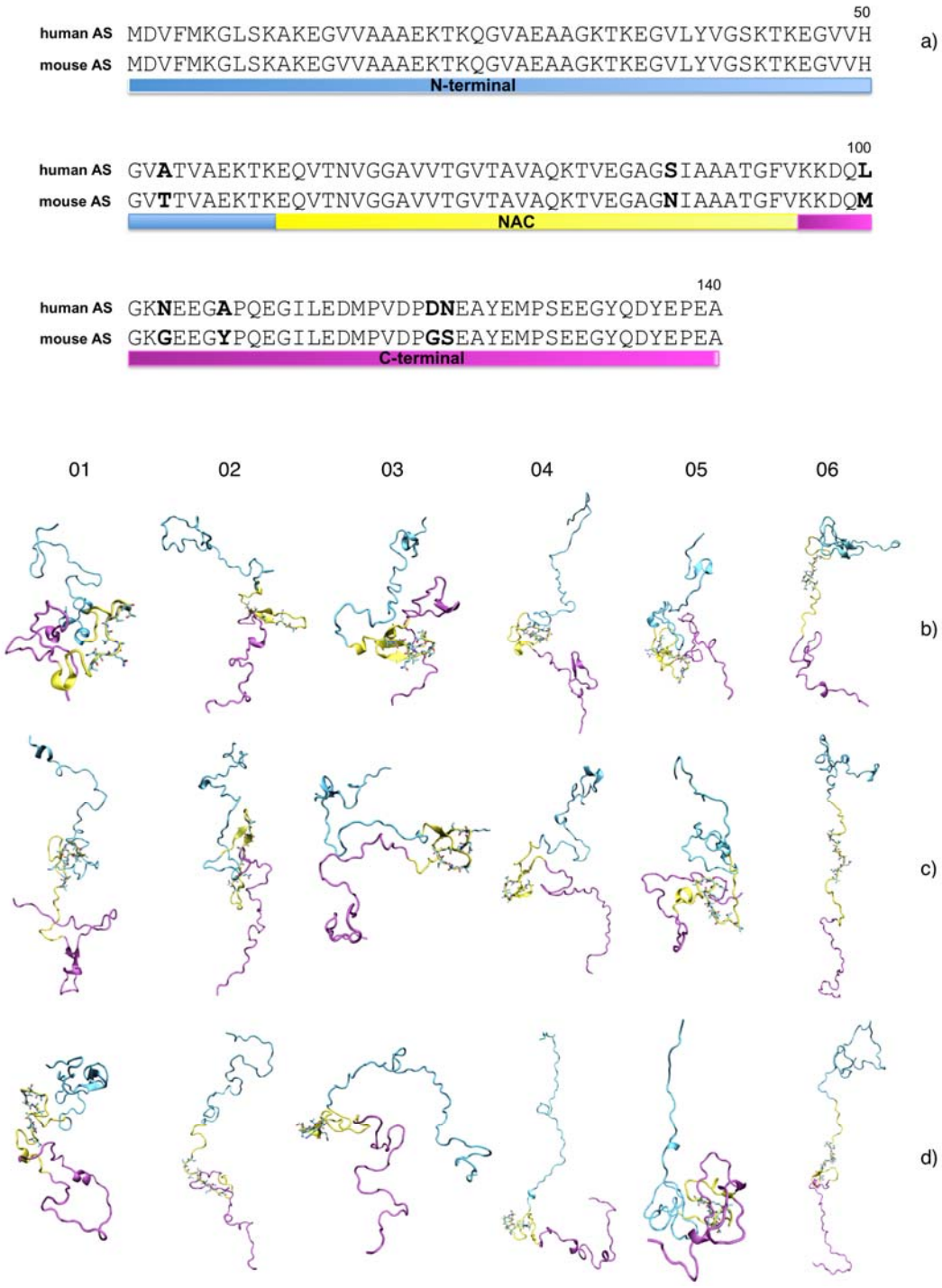
50
human AS MDVFMKGLSKAKEGVVAAAEKTKQGVAEAAGKTKEGVLYVGSKTKEGVVH
mouse AS MDVFMKGLSKAKEGVVAAAEKTKQGVAEAAGKTKEGVLYVGSKTKEGVVH
N-terminal
a)
100
human AS GVATVAEKTKEQVTNVGGAVVTGVTAVAQKTVEGAGSIAAATGFVKKDQL
mouse AS GVTTVAEKTKEQVTNVGGAVVTGVTAVAQKTVEGAGNIAAATGFVKKDQM
NAC
140
human AS GKNEEGAPQEGILEDMPVDPDNEAYEMPSEEGYQDYEPEA
mouse AS GKGEEGYPQEGILEDMPVDPGSEAYEMPSEEGYQDYEPEA
C-terminal
01
02
03
04
05
06
b)
c)
d)

Figure 2.

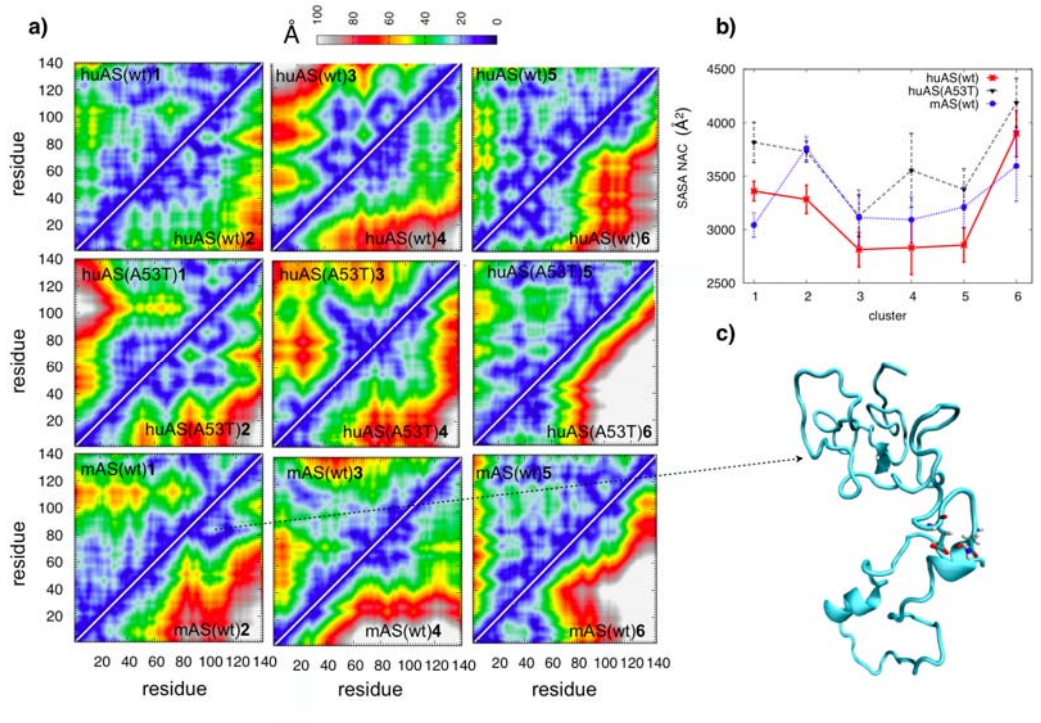
a)
Å
100
80
60
40
20
0
huAS(wt)1
huAS(wt)2
huAS(wt)3
huAS(wt)4
huAS(wt)5
huAS(wt)6
huAS(A53T)1
huAS(A53T)2
huAS(A53T)3
huAS(A53T)4
huAS(A53T)5
huAS(A53T)6
mAS(wt)1
mAS(wt)2
mAS(wt)3
mAS(wt)4
mAS(wt)5
mAS(wt)6
residue
20 40 60 80 100 120 140
b)
huAS(wt)
huAS(A53T)
mAS(wt)
SASA NAC (Å²)
4500
4000
3500
3000
2500
1 2 3 4 5 6
cluster
c)

Figure 3.

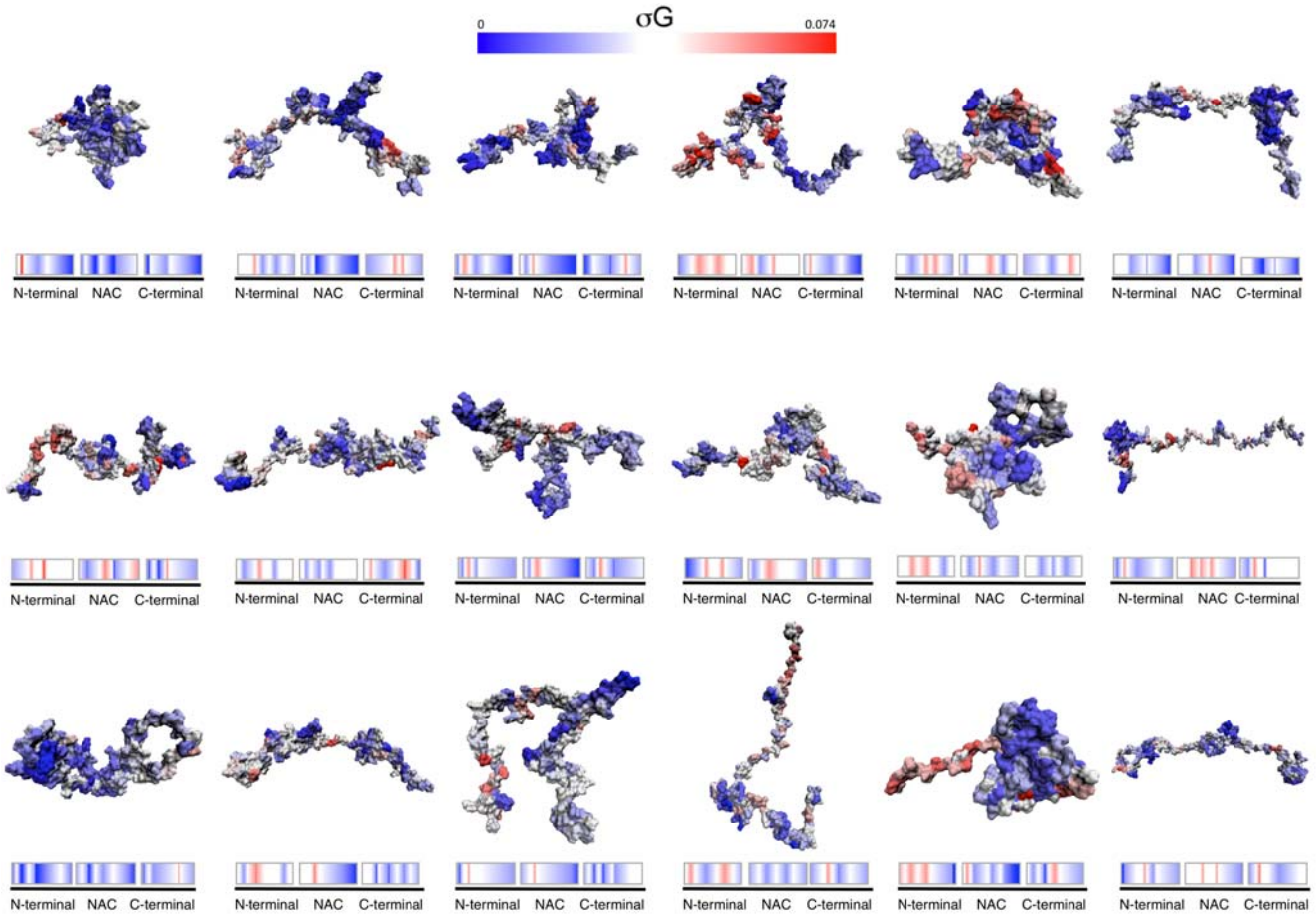

Graphics for the table of contents

Structural Role of Compensatory Aminoacid Replacements in the Alpha-Synuclein Protein

Valeria Losasso, Adriana Pietropaolo, Claudio Zannoni, Stefano Gustincich, Paolo Carloni

For Table of Contents Use Only